

# The Mechanism for Acetylcholine Receptor Inhibition by $\alpha$ -Neurotoxins and Species-Specific Resistance to $\alpha$ -Bungarotoxin Revealed by NMR

Abraham O. Samson,<sup>1</sup> Tali Scherf,<sup>2</sup>  
Miriam Eisenstein,<sup>2</sup> Jordan H. Chill,<sup>1</sup>  
and Jacob Anglister<sup>1,3</sup>

<sup>1</sup>Department of Structural Biology and

<sup>2</sup>Chemical Services

The Weizmann Institute of Science

Rehovot 76100

Israel

## Summary

The structure of a peptide corresponding to residues 182–202 of the acetylcholine receptor  $\alpha 1$  subunit in complex with  $\alpha$ -bungarotoxin was solved using NMR spectroscopy. The peptide contains the complete sequence of the major determinant of AChR involved in  $\alpha$ -bungarotoxin binding. One face of the long  $\beta$  hairpin formed by the AChR peptide consists of exposed non-conserved residues, which interact extensively with the toxin. Mutations of these receptor residues confer resistance to the toxin. Conserved AChR residues form the opposite face of the  $\beta$  hairpin, which creates the inner and partially hidden pocket for acetylcholine. An NMR-derived model for the receptor complex with two  $\alpha$ -bungarotoxin molecules shows that this pocket is occupied by the conserved  $\alpha$ -neurotoxin residue R36, which forms cation- $\pi$  interactions with both <sup>W</sup>149 and <sup>W</sup>55/<sup>W</sup>57 of the receptor and mimics acetylcholine.

## Introduction

The nicotinic acetylcholine receptor (AChR) is a ligand-gated cation channel activated upon binding of acetylcholine (ACh). It is a 290 kDa membranal glycoprotein found in muscle and neuronal tissues consisting of five homologous subunits in the stoichiometry of  $\alpha_2\beta\delta\gamma$  or  $\alpha_2\beta\delta\epsilon$  (Corringer et al., 2000; Karlin, 1993). Located on the postsynaptic surface of the neuromuscular junction, the AChR translates the chemical signal of ACh binding into an electrical one, leading to muscle contraction. The receptor has two ACh binding sites formed by the  $\alpha/\delta$  and  $\alpha/\gamma$  subunits (Blount and Merlie, 1989). The  $\alpha$  subunit of the muscle AChR ( $\alpha 1$ ) also contains a high-affinity binding site for antagonists such as  $\alpha$ -neurotoxins (Haggerty and Froehner, 1981).

$\alpha$ -bungarotoxin ( $\alpha$ -BTX) is a 74 amino acid, 8 kDa  $\alpha$ -neurotoxin derived from the venom of the snake *Bungarus multicinctus*. It binds to the postsynaptic muscle AChR with an  $IC_{50}$  value of  $3.5 \times 10^{-10}$  M (Wilson et al., 1988), competitively inhibiting ACh binding, thereby preventing the depolarizing action on postsynaptic membranes and blocking neuromuscular transmission. The major determinant involved in toxin binding was mapped to the segment <sup>W</sup>184-<sup>D</sup>200 which forms a  $\beta$  hairpin (Samson et al., 2001) ( $\alpha$ -BTX and AChR residues are designated by a superscript B (<sup>B</sup>X),  $\alpha 1$ ,  $\alpha 7$ ,  $\beta$ ,

or  $\delta$  (i.e. <sup>X</sup>), respectively, before the one letter amino acid code indicating the subunit type and the position in sequence). Sequence analysis has shown that resistance of certain species such as mongoose and cobra to  $\alpha$ -BTX is correlated with mutations in this region (Barchan et al., 1992).

In comparison to *Torpedo* AChR, which is homologous to muscle AChR, the neuronal AChR ( $\alpha 7$ -homopentamer) binds  $\alpha$ -BTX with 20-fold weaker affinity and short neurotoxins with five orders of magnitude weaker affinity (Servent et al., 1998).  $\alpha 7$  does not show any significant variations in its amino acid sequence among different species and even mongoose  $\alpha 7$  binds  $\alpha$ -BTX (Ariel et al., 1998). The peptide  $\alpha 7^{181-200}$  of chick neuronal AChR (IPGKRNESFYECCKEYPYD, the numbering of all peptides is according to alignment with  $\alpha 1$ ) binds  $\alpha$ -BTX with a dissociation constant of  $3 \times 10^{-5}$  M, three orders of magnitude higher than that for the  $\alpha 1^{187-200}$  peptide (Harel et al., 2001; Moise et al., 2002).

The three-dimensional solution structure of  $\alpha$ -BTX in complex with a 13 residue peptide, LP (MRYESSLK SYPD), selected from a phage-displayed random peptide library (Scherf et al., 1997) as well as that between  $\alpha$ -BTX and two peptides based on the library peptide and modified for higher affinity, HAP2 and HAP (WRYE ESSLEPYD and WRYE SLLPYD, respectively), were determined by NMR (HAP2) and X-ray crystallography (HAP) (Harel et al., 2001; Scherf et al., 2001). In the latter two structures, nine peptide residues were found to interact with  $\alpha$ -BTX. The high-affinity peptides are highly homologous to the major  $\alpha$ -BTX binding determinant of the  $\alpha 7$  subunit ( $\alpha 7^{187-200}$ ) with no insertion or deletions in the sequence, and their two structurally important proline residues are located at the same positions (Moise et al., 2002). Replacement of  $\alpha 7$  E187 and K194 with tryptophan and leucine, respectively, in the HAP peptides increased the affinity of the peptides to  $\alpha$ -BTX by three orders of magnitude. All other amino acids of the HAP peptides were identical to human  $\alpha 7$  or were conservatively replaced. Replacement of <sup>HAP</sup>R188 and <sup>HAP</sup>L194 by valine and proline as in the corresponding positions in the muscle  $\alpha 1$  resulted in at least one and two orders of magnitude lower affinity, respectively, for each replacement. Interestingly, <sup>W</sup>194 is conserved in species sensitive to  $\alpha$ -BTX and is replaced by leucine in both mongoose and cobra, which are resistant to  $\alpha$ -BTX, indicating that proline at position 194 is crucial for  $\alpha 1$  binding to  $\alpha$ -BTX. <sup>W</sup>188 is an invariant  $\alpha 1$  residue (Barchan et al., 1992). These findings indicate that the requirements for strong  $\alpha$ -BTX binding are considerably different for  $\alpha 1$  and HAP, the latter of which resembles  $\alpha 7$  (Kasher et al., 2001).

Recently, the structure of  $\alpha$ -BTX in complex with a peptide corresponding to residues  $\alpha 7^{181-200}$  of chick neuronal AChR was solved using NMR (Moise et al., 2002). The secondary structure of the peptide was not defined. Only four residues out of the 19 peptide residues were found to interact with  $\alpha$ -BTX, and both the intermolecular  $\beta$  sheet and the peptide  $\beta$  hairpin conformation previously observed for  $\alpha 1^{182-202}$  (Samson et al., 2001) and

<sup>3</sup>Correspondence: jacob.anglister@weizmann.ac.il

for HAP (Harel et al., 2001) and HAP2 (Scherf et al., 2001) were not observed for  $\alpha 7^{181-200}$ .

The structure of the whole AChR has not been solved yet at high resolution. Recently, the crystal structure of a snail ACh binding protein (AChBP) was determined (Brejc et al., 2001). This homopentamer shares 27% sequence identity with  $\alpha 7$ . Superposition of the toxin bound high-affinity peptide HAP on the analogous region of the AChBP located the binding site for  $\alpha$ -neurotoxins at the outer perimeter of the AChBP at the interface between two identical subunits (Harel et al., 2001). The molecular axis of the toxin was found to be perpendicular both to the 5-fold symmetry axis and to the tangent to the pentameric ring (the molecular axis of  $\alpha$ -BTX is defined here as the long axis of the second finger). Due to the perpendicular orientation, the contact area between the toxin and the receptor is only 760 Å<sup>2</sup>, not accounting for the extremely high affinity between the two proteins. Moreover, the superposition used resulted in numerous clashes between the toxin and the homopentameric AChBP that could potentially be relieved by elaborate modeling. The clashes prevented detailed analysis of the interactions between  $\alpha$ -BTX and the heteropentameric muscle AChR, and the interactions between the two proteins could be inferred only by analogy to the AChBP.

In the present study, we determined the solution structure of a complex between  $\alpha$ -BTX and a peptide corresponding to the segment  $\alpha 1^{182-202}$  containing the entire major ligand binding domain of *Torpedo*  $\alpha 1$ , including all residues previously found to be important for species-specific resistance to  $\alpha$ -BTX. The one residue insertion in the  $\alpha 1$  sequence in comparison to  $\alpha 7$  and a different location of the proline residues resulted in a  $\beta$  bulge within the  $\beta$  hairpin, not found in  $\alpha 7$ .  $\alpha 1^{K185}$ ,  $\alpha 1^{W187}$ ,  $\alpha 1^{Y189}$ , and  $\alpha 1^{P194}$ , found on the exposed face of the  $\alpha 1^{182-202}$   $\beta$  hairpin, interact extensively with  $\alpha$ -BTX, thus explaining all the natural mutations in  $\alpha 1$  leading to species-specific resistance to snake toxins. Using our NMR structure of  $\alpha$ -BTX/ $\alpha 1^{182-202}$  complex, we constructed a homology-based model of the extracellular domain of the AChR, AChR-EC, in complex with two toxin molecules. In this model,  $\alpha$ -BTX forms an angle of approximately 35° with the plane of the pentameric ring and a 37° angle with the tangent to the ring. This orientation considerably increases the contact area between AChR and  $\alpha$ -BTX. According to our model, more than 1800 Å<sup>2</sup> of the toxin surface are buried upon receptor binding, compared to a mere 760 Å<sup>2</sup> in the AChBP superposition (Harel et al., 2001), clearly in line with the high affinity to the receptor. The conserved  $\alpha$ -neurotoxin residue  $R36$  occupies the partially buried deep pocket for ACh, thus providing an explanation for the mechanism of AChR inhibition by snake  $\alpha$ -neurotoxins.

## Results

### Structure Determination

Structure determination by NMR is based on a large number of constraints on inter-proton distances obtained from the analysis of the NOESY spectrum and constraints on dihedral angles obtained from measurements of <sup>3</sup>J coupling constants (Wüthrich, 1986). A total of 522 long-range distance constraints were used in

the structure calculations of the  $\alpha$ -BTX/ $\alpha 1^{182-202}$  complex including 375 intra-toxin, 104 peptide/toxin, and 43 intra-peptide constraints. This is an order of magnitude more long-range distance constraints than those used by Hawrot and coworkers for a shorter  $\alpha 1$  peptide (Zeng et al., 2001). Torsion-angle constraints included 77  $\phi$ -angles and 41  $\chi_1$ -angles. Figure 1A shows the backbone superposition of 28 lowest energy structures of the complex that satisfy the experimental restraints with no NOE violations larger than 0.4 Å and no torsion angle violations exceeding 5°. The overall structure of the complex is well defined with rmsd values of 0.84 Å and 1.45 Å for the backbone and heavy atoms, respectively (excluding peptide terminal residues  $\alpha 1^{R182}$ - $\alpha 1^{G183}$  and  $\alpha 1^{I201}$ - $\alpha 1^{T202}$ ). The structure of the  $\beta$  strands is very well defined with rmsd values of 0.45 Å and 1.00 Å for the backbone and heavy atoms, respectively. The statistical data for the final set of structures are presented in Table 1.

The Ramachandran plot (not shown) of the mean structure of the complex suggests that the  $\phi$  and  $\psi$  angles of the structure predominantly occupy allowed regions. Only one residue is outside the allowed region, namely  $\alpha 1^{C192}$ . The  $\phi$  and  $\psi$  angles of  $\alpha 1^{C192}$  are distorted probably due to the vicinal disulfide bridge with  $\alpha 1^{C193}$ . Such disulfide bonds are rare in proteins due to their unusual strain in bond length and angle, suggesting that they must play an important role in agonist binding (Kao and Karlin, 1986).

### Structure of the Bound $\alpha$ -BTX

As shown in Figure 1B, the overall structure of  $\alpha$ -BTX consists of three long fingers and a C-terminal tail. Finger I forms a  $\beta$  hairpin with two antiparallel  $\beta$  strands consisting of residues  $BV2$ - $BT6$  and  $B^{111}$ - $BT15$ . Finger II consists of two antiparallel  $\beta$  strands,  $B^{L22}$ - $BD30$  and  $B^{G37}$ - $BA45$ . Residues  $B^{E56}$ - $BC60$  of finger III form a triple-stranded antiparallel  $\beta$  sheet with finger II to create the central core of the toxin. These motifs are present in many  $\alpha$ -neurotoxins (Tsetlin, 1999). The backbone rmsd values between  $\alpha$ -BTX complexed with  $\alpha 1^{182-202}$  and complexed with HAP2 and HAP (Harel et al., 2001; Scherf et al., 2001) are 1.81 Å and 1.65 Å, respectively, excluding the C-terminal segment  $B^{K70}$ - $B^{G74}$ , which does not seem to adopt a well-defined secondary structure.

The secondary structure of free  $\alpha$ -BTX was determined earlier (Basus et al., 1988). In the  $\alpha$ -BTX complex with  $\alpha 1^{185-196}$ , residues  $B^{W28}$  and  $B^{V39}$  located at the edge of  $\beta$  sheet of the second finger zip together upon peptide binding (Basus et al., 1993). In the present study of  $\alpha$ -BTX in complex with the longer  $\alpha 1^{182-202}$ , additional residues, namely  $B^{C29}$ - $BD30$  and  $B^{G37}$ - $B^{K38}$ , extend the  $\beta$  sheet, illustrating the importance of  $\alpha 1^{P197}$ - $\alpha 1^{D200}$  in stabilizing the complex.

### Structure of Bound $\alpha 1^{182-202}$

As already revealed in secondary structure determination of the bound peptide (Samson et al., 2001),  $\alpha 1^{182-202}$  adopts a  $\beta$  hairpin conformation, consisting of two antiparallel  $\beta$  strands formed by residues  $\alpha 1^{H186}$ - $\alpha 1^{T191}$  and  $B^{Y198}$ - $B^{D200}$  (Figure 2A) and a six residue connecting loop made of  $\alpha 1^{C192}$ - $\alpha 1^{P197}$  (CCPDTP) rigidified by the disulfide bond and two prolines. The first three residues

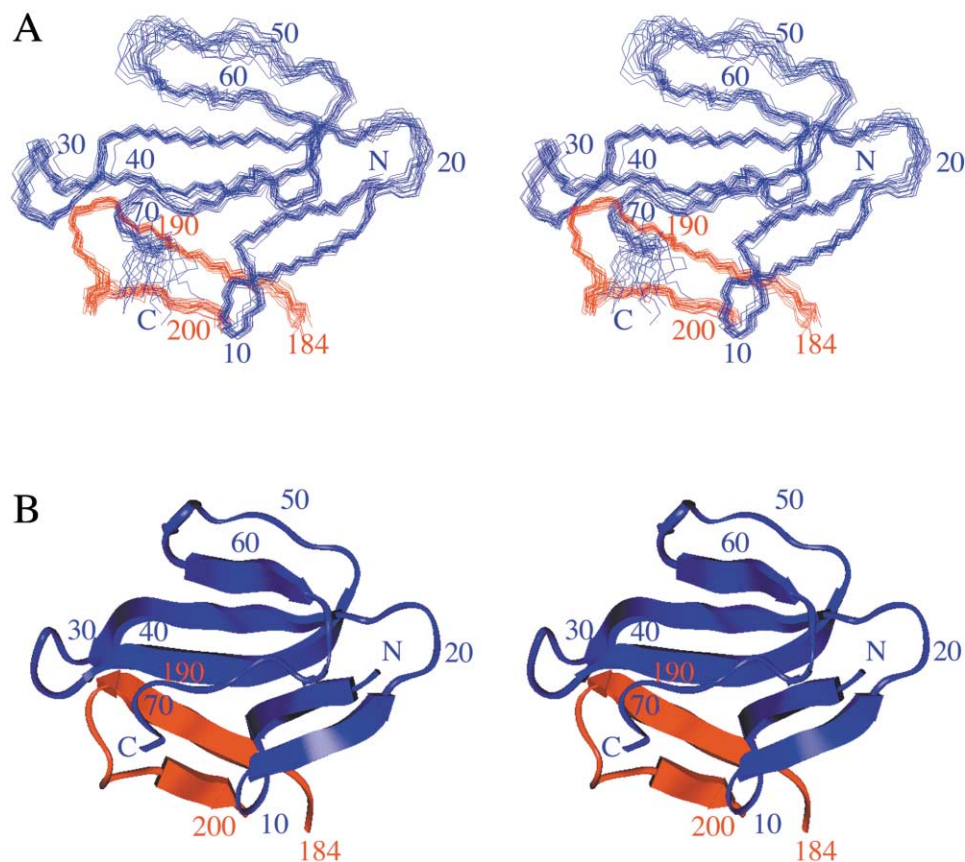


Figure 1. A Stereo View of the  $\alpha$ -BTX/ $\alpha^1$ <sup>182-202</sup> Complex

Only the peptide segment  $\alpha^1$ W184- $\alpha^1$ D200, which exhibits a converged structure, is shown. N and C denote the termini of the toxin (blue) and the peptide (red) and each tenth residue is numbered. (A) Backbone superposition of 28 lowest energy structures. (B) A ribbon diagram of the energy-minimized average structure. All figures were prepared using Insight II and MOLMOL (Koradi et al., 1996).

of the elongated  $\beta$  strand  $\alpha^1$ H186- $\alpha^1$ T191 interact with the second  $\beta$  strand of  $\alpha^1$ <sup>182-202</sup>,  $\alpha^1$ Y198- $\alpha^1$ D200, thus closing the  $\beta$  hairpin, while the last three residues of the first strand, namely  $\alpha^1$ Y189- $\alpha^1$ T191, associate with the toxin residues  $^B$ K38- $^B$ V40, to form an intermolecular  $\beta$  sheet

(Figure 2A). The upper face of the  $\beta$  hairpin is formed by the sidechains of residues  $\alpha^1$ K185,  $\alpha^1$ W187,  $\alpha^1$ Y189,  $\alpha^1$ P194,  $\alpha^1$ P197, and  $\alpha^1$ L199, while the lower face is formed by the sidechains of  $\alpha^1$ H186,  $\alpha^1$ V188,  $\alpha^1$ Y190,  $\alpha^1$ C192,  $\alpha^1$ C193,  $\alpha^1$ Y198, and  $\alpha^1$ D200, thus stabilizing the  $\beta$  hairpin conformation through mostly hydrophobic interaction (Figure 2A).

Table 1. NMR Constraints and Structural Statistics for 28 Structures of the  $\alpha$ -BTX/ $\alpha^1$ <sup>182-202</sup> Complex

NMR Distance Constraints	
Total constraints	1673
Long range in $\alpha$ -BTX ( $ i - j  > 4$ )	375
Long range in peptide ( $ i - j  > 4$ )	43
Toxin/peptide	134
Torsion Angle Constraints	
$\phi$ angles constraints	77
$\chi_1$ angles constraints	41
NOE Violations (Å)	
Maximum individual violation	0.40
Rmsd of NOE violations	0.033 $\pm$ 0.002
Deviations from Ideal Covalent Geometry	
Bonds lengths (Å)	0.0041 $\pm$ 0.0002
Bond angles (°)	0.6127 $\pm$ 0.0236
Improper angles (°)	0.5268 $\pm$ 0.0319
Mean Rmsd Values (Å)	
Backbone atoms	0.84
All heavy atoms	1.45
Backbone atoms of secondary structure	0.45
Backbone atoms of peptide (184-200)	0.43

The corresponding region of AChBP (KKNSVTYSCC PEAYEDV, residues 179-194) was found to adopt a  $\beta$  hairpin conformation, in which Ser<sup>186</sup>-Cys<sup>187</sup> form a turn (Brejc et al., 2001). Backbone superposition of the  $\alpha$ -BTX bound AChR segments  $\alpha^1$ K185- $\alpha^1$ Y190 and  $\alpha^1$ Y198- $\alpha^1$ L199 over that of the corresponding AChBP region resulted in an rmsd of 1.4 Å (Figure 2B), a deviation originating mostly from the one residue insertion  $\alpha^1$ P194 in the AChR sequence. The two prolines ( $\alpha^1$ P194,  $\alpha^1$ P197) of  $\alpha^1$ <sup>182-202</sup> break the  $\beta$  structure and produce a  $\beta$  bulge consisting of the segment  $\alpha^1$ P194- $\alpha^1$ P197. The second  $\beta$  strand in AChBP extends beyond its three residue counterpart in  $\alpha^1$ <sup>182-202</sup> ( $\alpha^1$ Y198- $\alpha^1$ D200).

#### $\alpha^1$ <sup>182-202</sup>/ $\alpha$ -BTX Binding Interactions

Surrounded by the toxin,  $\alpha^1$ <sup>182-202</sup> fits snugly into the  $\alpha$ -BTX binding site. As shown in Figure 2C and Table 2, 12  $\alpha^1$ <sup>182-202</sup> residues interact with 19 toxin residues. The sidechains of  $\alpha^1$ K185,  $\alpha^1$ W187, and  $\alpha^1$ Y189 interact

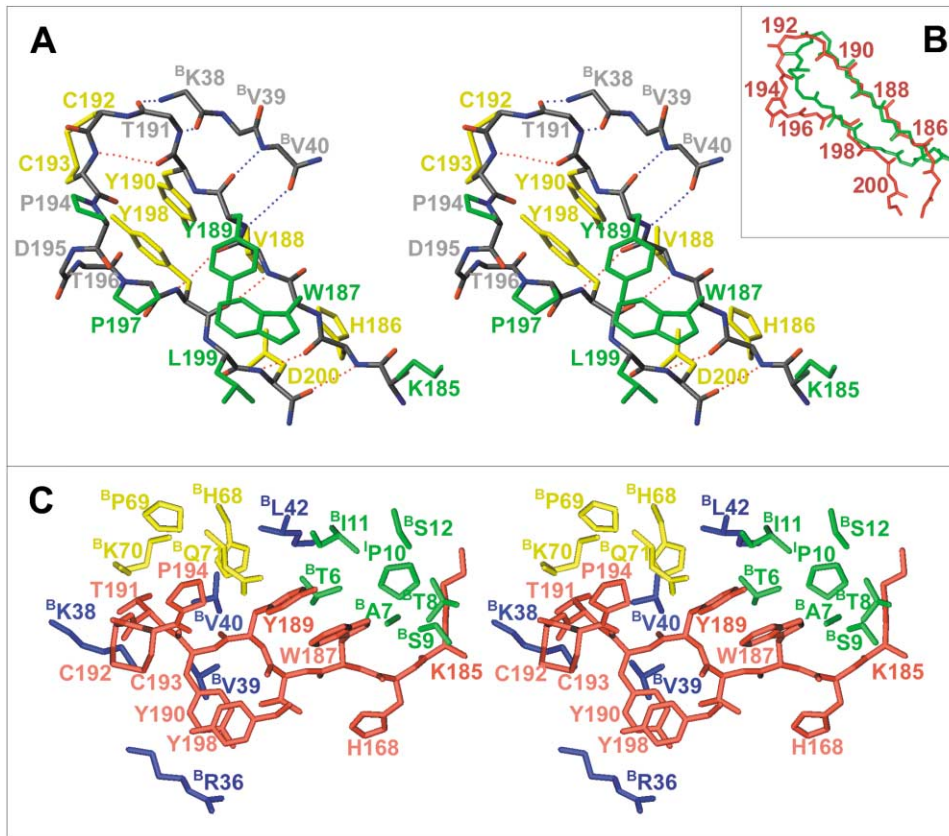


Figure 2. The Structure and Interactions of the  $\alpha$ -BTX Bound  $\alpha 1^{182-202}$

(A) Stereo representation of the hydrogen bonding and intramolecular side chain interactions of the bound  $\alpha 1^{182-202}$ . Side chains pointing out from the page are in green and side chains pointing inwards are in yellow. Intramolecular hydrogen bonds within the peptide and intermolecular hydrogen bonds with  $^B K38$ - $^B V40$  are in red and blue dotted lines, respectively. (B) Superposition of the  $^{\alpha 1} H186$ - $^{\alpha 1} D200$  segment and the corresponding segment of AChBP (N181-D194). Shown are the backbone atoms of  $\alpha 1^{182-202}$  (in red) and of the corresponding AChBP segment (in green). (C) A stereo representation of side chain interactions of  $\alpha 1^{182-202}$  with  $\alpha$ -BTX. The peptide (in red) interacts with the first finger (in green), second finger (in blue), and C terminus (in yellow) of  $\alpha$ -BTX.

through mostly hydrophobic interaction with residues  $^B T6$ - $^B S12$  of the first finger of  $\alpha$ -BTX. Peptide residues  $^{\alpha 1} Y189$ - $^{\alpha 1} T191$  interact with residues  $^B K38$ - $^B V40$  of the toxin  $\beta$  sheet core through an intermolecular  $\beta$  sheet involving four hydrogen bonds (Figure 2A). Hydrophobic interactions between  $^{\alpha 1} Y189$  and  $^B V40$  on the upper side of the  $\beta$  hairpin and between  $^{\alpha 1} Y190$  and  $^B V39$  on the lower side of the  $\beta$  hairpin help stabilize the intermolecular  $\beta$  sheet. The sidechains of tyrosines  $^{\alpha 1} Y190$  and  $^{\alpha 1} Y198$  on the lower side of the  $\beta$  hairpin interact with  $^B R36$  of the toxin's second finger, a highly conserved toxin residue found to be important for toxin binding to AChR (see below). Finally, residues  $^{\alpha 1} Y189$ ,  $^{\alpha 1} T191$ ,  $^{\alpha 1} C192$ , and  $^{\alpha 1} P194$  interact through mostly hydrophobic interaction with residues  $^B H68$ - $^B Q71$  at the C terminus of the toxin (Figure 2C). Residues  $^{\alpha 1} K185$ ,  $^{\alpha 1} W187$ ,  $^{\alpha 1} Y189$ ,  $^{\alpha 1} Y190$ ,  $^{\alpha 1} T191$ ,  $^{\alpha 1} C192$ , and  $^{\alpha 1} P194$  are the strongest contributors to the contact surface between  $\alpha 1^{182-202}$  and the toxin.

#### A Model for AChR-EC

The sequence identity between AChBP and each AChR-EC subunit is only 19%–24% (Brejc et al., 2001). Nevertheless, the sequence alignment of the AChBP monomer and each of the AChR-EC subunits shows a good fit

with almost no gaps over the entire sequence (Figure 3H). The highest similarity is found in the secondary structure elements. The cysteine pair  $^{\alpha 1} C128$  and  $^{\alpha 1} C142$  is conserved in all AChR-EC subunits, while the vicinal  $^{\alpha 1} C192$  and  $^{\alpha 1} C193$  pair is conserved in  $\alpha$  subunits only. Replacement of the sidechains of AChBP by those of AChR-EC in the structurally conserved regions (see Experimental Procedures) resulted in no steric collisions. The loops produced few molecular clashes, which were alleviated by manually assigning alternative rotamers to the sidechains of colliding residues. The resulting homology-based model of the heteropentameric AChR-EC is shown in Figure 3.

According to our model, the ACh binding pocket, previously identified in the crystal structure of the homopentameric AChBP (Brejc et al., 2001), is located at the interface between the  $\alpha 1\gamma$  or  $\alpha 1\delta$  subunits and is lined by aromatic and hydrophobic residues:  $^{\alpha 1} Y93$ ,  $^{\alpha 1} W149$ ,  $^{\alpha 1} Y190$ , and  $^{\alpha 1} Y198$  of the  $\alpha 1$  subunit as well as  $^{\gamma} W55$ / $^{\delta} W57$  and  $^{\gamma} L119$ / $^{\delta} L121$ . Different residues are found in the corresponding positions in the other subunits, accounting for the absence of ligand binding.

#### The Ion Channel

AChBP is a soluble protein found in the synaptic cleft, where it modulates synaptic transmission. It consists of

Table 2. Interactions between  $\alpha$ -BTX and the AChR Various Subunits

$\alpha$ -BTX	$\alpha$	$\gamma$	$\delta$
T5	<i>Y189</i>		
T6	<i>W187</i>	<i>Y189</i>	
A7	<i>K185</i>	H186	<i>W187</i>
<u>T8</u>	<i>K185</i>	<u><i>W187</i></u>	L199
<u>S9</u>	<i>W187</i>	L199	
<u>P10</u>	<i>W187</i>	<i>Y189</i>	
I11	<i>W187</i>	<i>Y189</i>	
S12	<i>K185</i>		
<u>K26</u>		W170	<u>E176</u>
M27	T191		I177 I178 I179 <u>E182</u>
W28		E169 W170 I171 H172 P175 E176	E182 A183
C29		A167 V168 E169 W170	D171 A183
D30	Y190	T36 W55 I171	D171 Y172 P173 A183
<u>A31</u>	Y190	L119 T36 W55	<u>T38</u> W57 <u>D171</u>
F32		K34 T36 A162	T164
<u>C33</u>		T36 A162 A167 V168 <u>R189</u>	D165 G169 K170 D171 K195
<u>S34</u>		<u>K34</u> L35 T36 R189	<u>S36</u> L37 T38 L39 <u>K170</u> <u>D171</u> K195
<u>S35</u>		K34 T36 <u>W55</u> E57 L119	S36 L37 T38 <u>W57</u> D59 L121 M163
<u>R36</u>	<u>W149</u> <i>Y190</i> <i>Y198</i>	W55 E57 L119	T38 W57 D59 L121
G37	Y190 <i>T191</i>		
<u>K38</u>	<i>Y190</i> <u><i>T191</i></u>	A167	<u>D165</u>
<u>V39</u>	<i>Y189</i> <u><i>Y190</i></u> <i>T191</i>	I171 H172	
<u>V40</u>	<u><i>Y189</i></u> <i>Y190</i> <i>T191</i> <i>C192</i>		
E41	<i>V188</i>	H172 P175	W176
L42	<i>Y189</i>		
C48			I178
P49			I178
K51		W170	E182
<u>K52</u>		<u>E169</u> W170	<u>D180</u>
P53		E166	
Y54		E166 A167 V168 E169 I186 R187	I167 D168 K170
E55		E169 W170	E182
H68	<i>Y189</i> <i>T191</i> <i>C192</i>		
P69	<i>T191</i> <i>C192</i>		
K70	<i>T191</i> <i>C192</i> <i>P194</i>		
Q71	<i>C192</i> <i>P194</i>		

Underlined are residues that form intermolecular toxin-receptor hydrogen bonds.  
Interactions between the toxin and the  $\alpha$ -subunit that were detected by NMR are in italics.

five identical subunits arranged as a doughnut to form a central pore. This protein is not an ion channel and therefore does not require a negatively charged duct along its 5-fold axis. Indeed, the electrostatic potential map of AChBP, shown in Figures 3A and 3B, presents a slightly positively charged cavity on one side (3A) and a slightly negative cavity on the other side (3B). On the other hand, the heteropentameric AChR forms a strongly negative duct (Figures 3C and 3D), which measures 1–1.5 nm in radius, and 5 nm in height. Several residues lining the inner perimeter of the AChR channel duct are different from those of the AChBP. Uncharged amino acids of the AChBP are mutated to negatively charged ones (i.e., S79 to  $\alpha^1$ D/ $\gamma$ , $\delta$ E, S80 to  $\alpha^1$ , $\beta$ D, S93 to  $\alpha^1$ , $\beta$ , $\gamma$ , $\delta$ D) and positively charged to negative or neutral residues (i.e., H69 to  $\alpha^1$ D/ $\gamma$ , $\delta$ E/ $\beta$ A, K94 to  $\alpha^1$ D/ $\gamma$ , $\delta$ Q/ $\beta$ S).

#### NMR-Derived Model of the $\alpha$ -BTX/AChR-EC Complex

The  $\beta$  hairpin ( $\alpha^1$ K185- $\alpha^1$ D200, shown in red in Figure 3E) in the NMR structure of the  $\alpha$ -BTX/ $\alpha^1$ <sup>182-202</sup> complex was superimposed on the corresponding  $\beta$  hairpin in the AChR-EC model. The  $\beta$  hairpin in the AChR model was then exchanged with the NMR structure of the entire  $\alpha$ -BTX/ $\alpha^1$ <sup>182-202</sup> complex. This procedure better defined the  $\beta$  hairpin conformation in the AChR model since the

NMR structure of this entire segment was used instead of a model based on AChBP, which has one deletion in this segment. The exchange with the whole  $\alpha$ -BTX/ $\alpha^1$ <sup>182-202</sup> complex automatically dictated the position of the toxin relative to the receptor, thus generating an NMR-derived model for the  $\alpha$ -BTX/AChR-EC complex (Figures 3F and 3G). A steric clash observed between the sidechain of  $^{\beta}$ S34 and the receptor was resolved by energy minimization, allowing movement of only three residues ( $^{\beta}$ C33- $^{\beta}$ S35). Several steric clashes between the sidechains of  $^{\gamma}$ 168- $^{\gamma}$ 174 ( $^{\delta}$ 169- $^{\delta}$ 180 in the  $\delta$  subunit) and  $\alpha$ -BTX were eliminated by dynamics and energy minimization.

$\alpha$ -BTX forms an angle of approximately 35° with the plane of the pentameric ring of AChR and a 37° angle with the tangent to the ring (Figures 3F and 3G). In contrast, the superimposed model located  $\alpha$ -BTX in the plane of the pentameric ring and perpendicular to the tangent to the AChBP ring (Harel et al., 2001). The different angular orientation of  $\alpha$ -BTX in the AChR model dramatically increases its contact area with the receptor by a factor of ~2.5 (see below).

The most striking feature of the NMR-derived model of the AChR/ $\alpha$ -BTX complex is the ACh binding site occupied by  $^{\beta}$ R36 (Figures 4A and 4B), which mimics ACh (Figure 4C). The majority of the receptor residues



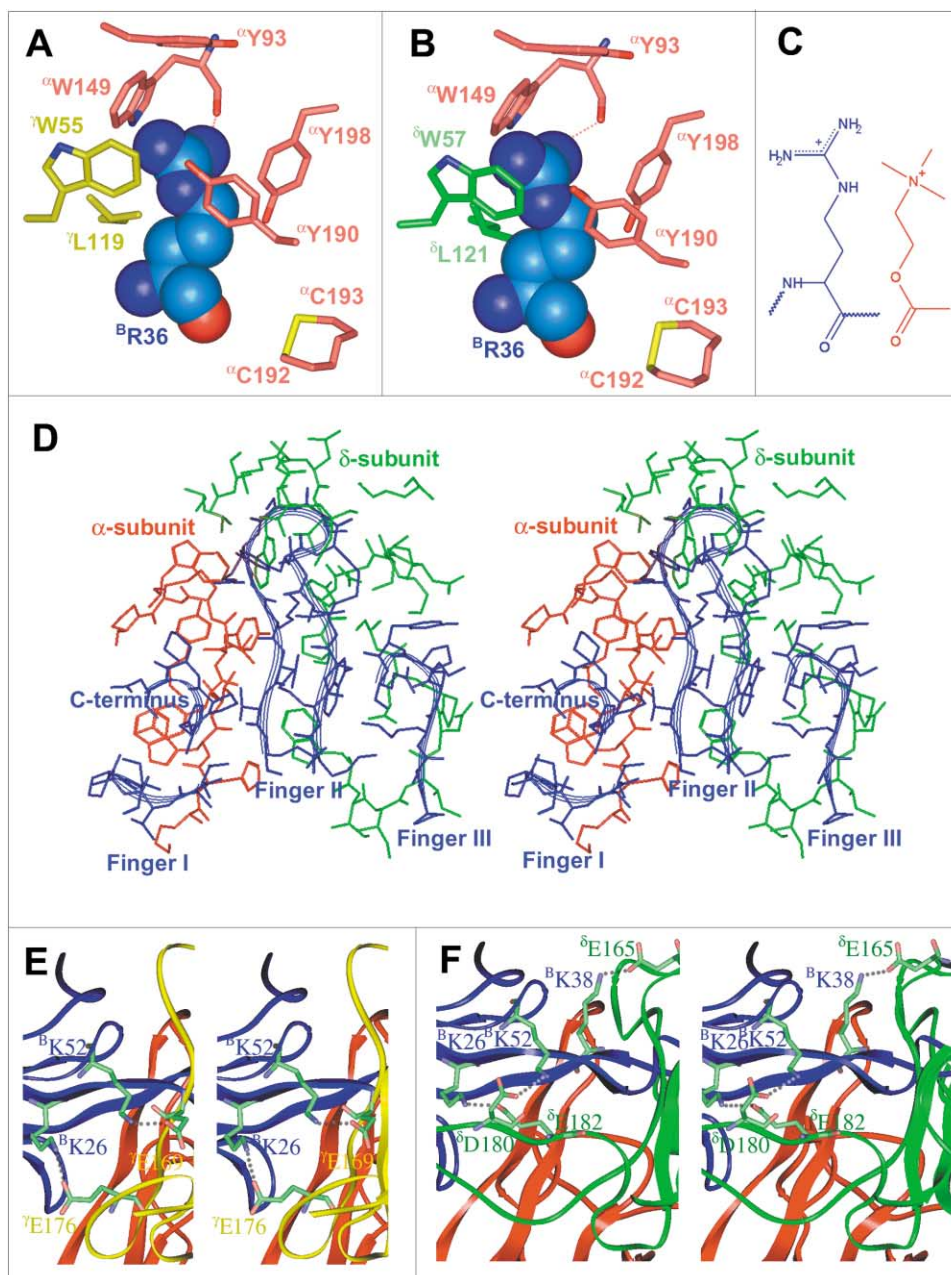


Figure 4. Interactions of  $\alpha$ -BTX with AChR-EC in the NMR-Derived Model

(A) Interactions of  $\alpha$ -BTX  $\beta^1$ R36 (blue) in the ACh binding pocket of AChR at the interface between the  $\alpha^1$  and  $\gamma$  subunits and (B) at the interface between the  $\alpha^1$  and  $\delta$  subunits. Residues of the  $\alpha^1$ ,  $\gamma$ , and  $\delta$  subunit are presented in pink, yellow, and green, respectively. (C) Structural comparison between ACh (red) and the arginine residue (blue). (D) Stereo view of the binding interface of the toxin with the  $\alpha^1$  and  $\delta$  subunits. Residues of the toxin first finger, C terminus, second finger, and third finger are presented from left to right in blue ribbons. Residues of the  $\alpha^1$  and  $\delta$  subunits are shown in red and green, respectively. The three figures and C-terminal of  $\alpha$ -BTX and  $\alpha$ AChR subunits are denoted. (E) Electrostatic interactions between  $\alpha$ -BTX and the  $\gamma$  subunit. A stereo representation of the ribbon diagrams of the  $\alpha^1$  (in red) and  $\gamma$  subunit (in yellow) interacting with the toxin (in blue). The salt bridges  $\gamma^1$ E169- $\beta^1$ K52 and  $\gamma^1$ E176- $\beta^1$ K26 are indicated by dashed lines. (F) The corresponding interactions of  $\alpha$ -BTX with the  $\delta$  subunit. A stereo representation of the ribbon diagrams of the  $\alpha^1$  (in red) and  $\delta$  subunit (in green) interacting with the toxin (in blue). The salt bridges  $\beta^1$ K26- $\delta^1$ E182,  $\beta^1$ K38- $\delta^1$ E165, and  $\beta^1$ K52- $\delta^1$ D180 are indicated by dashed lines.

site and its interaction with  $\alpha$ -BTX is given in Figure 4D. A summary of all the interactions between  $\alpha$ -BTX and AChR is given in Table 2. Intermolecular hydrogen bonds in the NMR-derived model are indicated as well (Table 2). Almost all the interactions of the  $\alpha^1$  subunit with the toxin arise from residues  $\alpha^1$ K185- $\alpha^1$ L199, the only

exception being the interaction of  $\alpha^1$ W149 with  $\beta^1$ R36. The first finger of the toxin interacts with the  $\alpha^1$  subunit only. The long second finger of  $\alpha$ -BTX penetrates deeply into the interface between the  $\alpha^1\gamma$  and the  $\alpha^1\delta$  subunits, and residues  $\beta^1$ K26- $\beta^1$ E41 ( $\beta^1$ R36 included) interact extensively with both subunits but mostly with the  $\gamma$  and  $\delta$

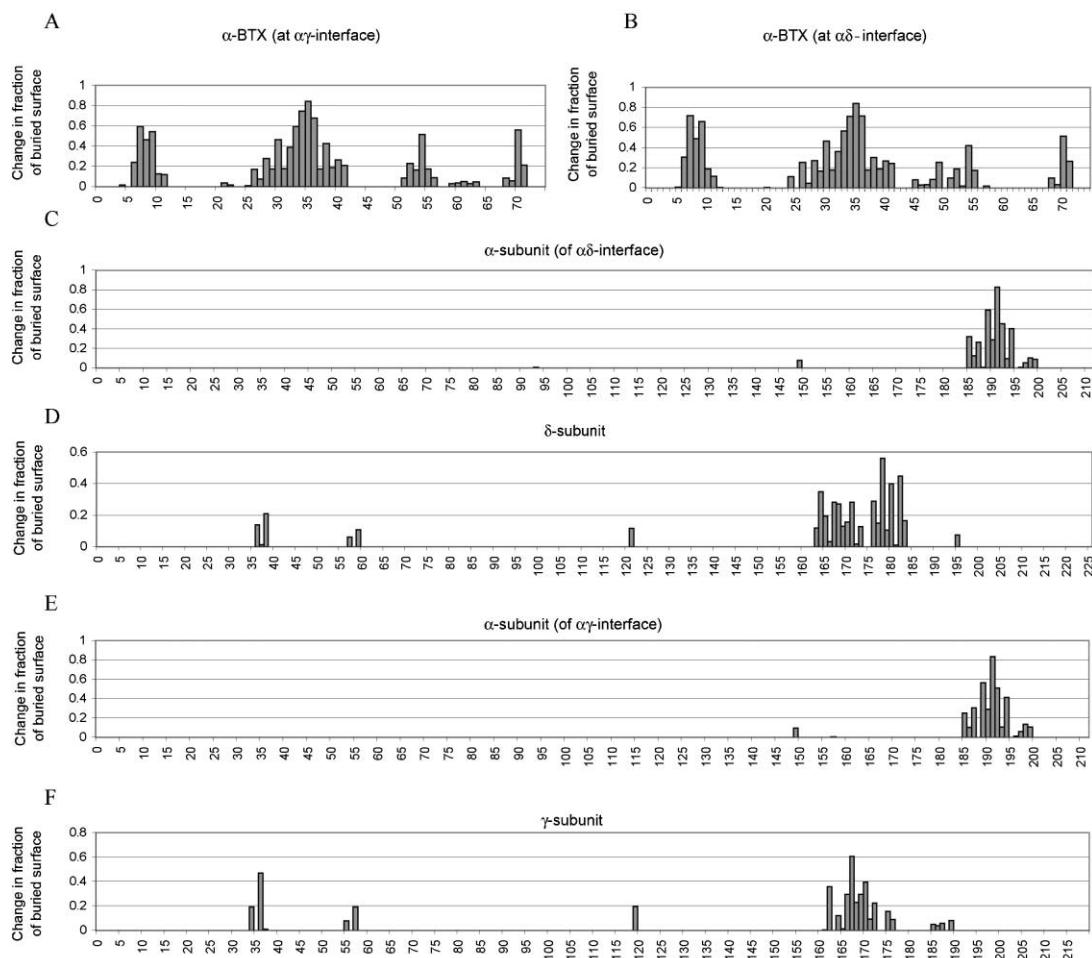


Figure 5. Fraction of Buried Surface upon Complex Formation of the AChR-EC and  $\alpha$ -BTX

Fractional solvent accessibility of each amino acid residue was calculated separately for the unbound receptor and toxin as well as for their complex. Bars correspond to the difference between the free and bound fractional solvent accessibility of every residue. Values of the two  $\alpha$ -BTX molecules are shown in (A) and (B), and values of the receptor subunits are presented in the (C)  $\alpha$ 1 subunit at the  $\alpha$ 1 $\delta$  interface, (D)  $\delta$  subunit, (E)  $\alpha$ 1 subunit at the  $\alpha$ 1 $\gamma$  interface, and (F)  $\gamma$  subunit. The solvent accessibility was calculated using Insight II (Accelrys).

subunits. The third finger interacts with the  $\gamma$  and  $\delta$  subunits and the C terminus of the toxin interacts only with the  $\alpha$ 1 subunit. Two buried intermolecular salt bridges are formed with the  $\gamma$  subunit ( $^{\text{B}}\text{K26}$ - $^{\text{Y}}\text{E176}$  and  $^{\text{B}}\text{K52}$ - $^{\text{Y}}\text{E169}$ ) and three buried salt bridges are formed with the  $\delta$  subunit ( $^{\text{B}}\text{K26}$ - $^{\text{D}}\text{E182}$ ,  $^{\text{B}}\text{K38}$ - $^{\text{D}}\text{E165}$ , and  $^{\text{B}}\text{K52}$ - $^{\text{D}}\text{D180}$ ) as shown in Figures 4E and 4F. The additional buried salt bridge formed between  $\alpha$ -BTX and the  $\delta$  subunit may explain the higher affinity of  $\alpha$ -BTX to the binding site formed by the  $\alpha$ 1 and  $\delta$  subunits.

Figure 4D illustrates how extensive the interactions between  $\alpha$ -BTX and AChR are. Upon binding AChR, 37% (1869  $\text{\AA}^2$ ) and 34% (1745  $\text{\AA}^2$ ) of the toxin surface (5013  $\text{\AA}^2$ ) become buried at the  $\alpha$ 1 $\delta$  and  $\alpha$ 1 $\gamma$  interfaces, respectively (Figures 5A and 5B). The buried surface area of the toxin is unusually large in comparison to other protein-protein complexes and explains the very tight binding between  $\alpha$ -BTX and AChR. The additional contact area of 124  $\text{\AA}^2$  is consistent with the higher affinity of the  $\alpha$ 1 $\delta$  binding site. Figures 5C–5F show the contribution of AChR residues to the binding. Most of

the AChR interactions with  $\alpha$ -BTX are formed by single loops in the  $\alpha$ 1,  $\gamma$ , and  $\delta$  subunits (185–200, 162–177, and 163–182, respectively). At the high-affinity binding site, 791  $\text{\AA}^2$  of the  $\alpha$ 1 subunit and 870  $\text{\AA}^2$  of the  $\delta$  subunits are buried upon  $\alpha$ -BTX binding. At the lower affinity binding site, 784  $\text{\AA}^2$  of the  $\alpha$ 1 subunit and 766  $\text{\AA}^2$  of the  $\gamma$  subunit are buried upon  $\alpha$ -BTX binding.

## Discussion

### The $\alpha$ 1<sup>182-202</sup> Peptide Mimics the Corresponding Region of AChR

In this study, the three-dimensional structure of the major neurotoxin binding determinant of  $\alpha$ 1 in complex with  $\alpha$ -BTX was determined by NMR. This study emphasizes the importance of selecting the appropriate length of the  $\alpha$ 1 peptide prior to structure elucidation. Shorter peptides would not have contained all residues contributing to  $\alpha$ -BTX binding or maintained the proper  $\beta$  hairpin fold, while longer peptides lead to aggregation. By first mapping the  $\alpha$ 1 determinant involved in  $\alpha$ -BTX bind-

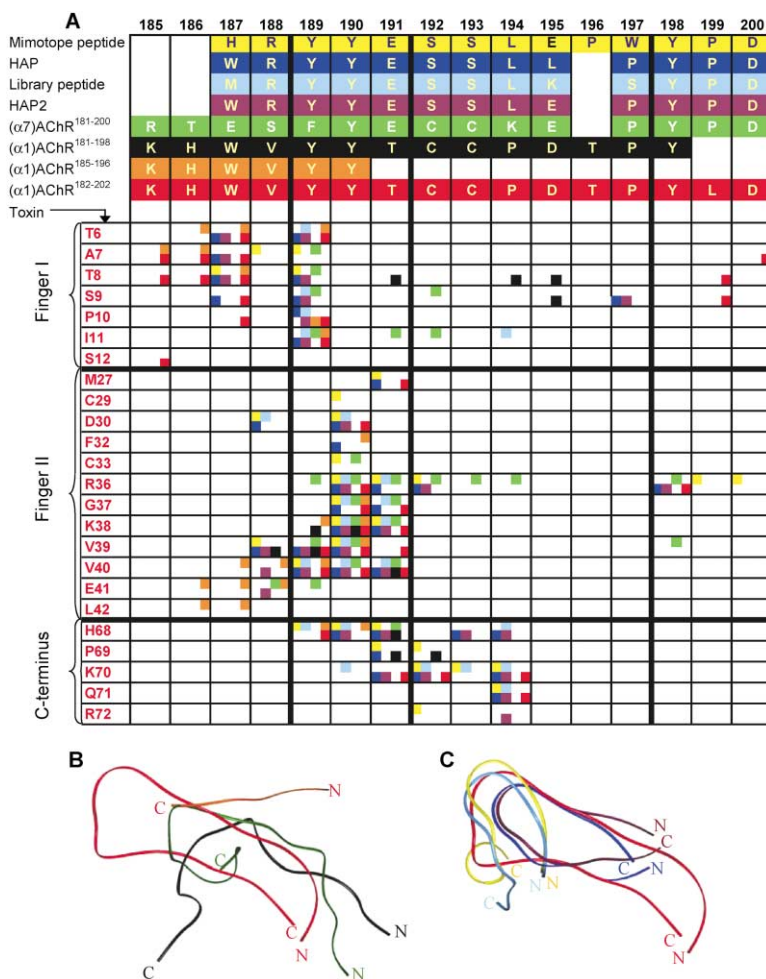


Figure 6. Comparison of the Different  $\alpha$ -BTX/Peptide Complexes

(A) Comparison of the interactions between  $\alpha$ -BTX and its bound peptide in different complexes. The sequences of the peptides are given on top of the figure. The interactions are indicated by colored boxes, each color corresponding to a different peptide. Heavy atoms less than 4 Å apart were considered as interacting. Distances were calculated using Insight II (Accelrys). (B) Superposition of a ribbon diagram of the NMR structures of  $\alpha 1^{182-202}$ ,  $\alpha 1^{185-196}$ ,  $\alpha 1^{181-198}$ , and  $\alpha 7^{181-200}$ . (C) Superposition of a ribbon diagram of the structure of  $\alpha 1^{182-202}$ , mimotope peptide, library peptide, HAP, and HAP2. The color coding for (A), (B), and (C) is as follows: mimotope peptide in yellow (Scarselli et al., 2002), HAP in dark blue (Harel et al., 2001), library peptide in light blue (Scherf et al., 1997), HAP2 in brown (Scherf et al., 2001),  $\alpha 7^{181-200}$  in green (Moise et al., 2002),  $\alpha 1^{181-198}$  in black (Zeng et al., 2001),  $\alpha 1^{185-196}$  in orange (Basus et al., 1993), and  $\alpha 1^{182-202}$  in red (present study).

ing (Samson et al., 2001), we obtained the optimal length of the peptide.

The  $\beta$  hairpin structure of  $\alpha 1^{182-202}$  bound to  $\alpha$ -BTX emulates that of the corresponding region in  $\alpha 1$  bound to  $\alpha$ -BTX. Designed by nature to bind to the corresponding segment of muscle  $\alpha 1$ , the  $\alpha$ -BTX binding site serves as a template and forces the flexible  $\alpha 1^{182-202}$  peptide to fold into a conformation similar to that of native  $\alpha 1$ . The assumption that the bound  $\alpha 1^{182-202}$  folds into its native structure is supported by the good agreement with the structure of AChBP, showing that the corresponding region in AChBP forms a  $\beta$  hairpin. As shown in Figures 6A and 6B, shorter  $\alpha 1$  peptides (Basus et al., 1993; Zeng et al., 2001) differ considerably from each other and from  $\alpha 1^{182-202}$  in their interactions and conformation. Strangely, the interactions of the N and C termini halves of the  $\alpha 1$  peptide are exchanged in  $\alpha 1^{181-198}$  (Zeng et al., 2001) in comparison to both  $\alpha 1^{185-196}$  (Basus et al., 1993) and  $\alpha 1^{182-202}$  (Figure 6).

The library-derived and the HAP peptides were selected on the basis of high affinity to  $\alpha$ -BTX. This selection may compromise the most important function of this determinant, i.e., ACh binding, and alter the conformation of the peptide to optimize the interaction with  $\alpha$ -BTX. This is especially evident in the lead library peptide (Scherf et al., 2001) and its derivative (Scarselli et

al., 2002), which form a globular conformation rather than a  $\beta$  hairpin. As shown in Figure 6A only the interactions of Y189, Y190, E191, and L194 in these two peptides (Scherf et al., 2001; Scarselli et al., 2002) are similar to those of the corresponding residues in  $\alpha 1^{182-202}$ . Therefore, although the library-derived peptide and the HAP peptides can serve as a better template for antidotes against snake  $\alpha$ -neurotoxins in comparison with  $\alpha 1^{182-202}$ , it is dubious whether they can accurately mimic the structure and interactions of  $\alpha 1^{182-202}$ .

The deletion at position 196, the location of the two prolines, and the high sequence homology potentially make the HAP peptides similar in conformation to  $\alpha 7$  rather than  $\alpha 1$ . The difference between the HAP peptide and  $\alpha 1$  is further emphasized by the observation that <sup>HAP</sup>L194 contributes significantly to the binding to  $\alpha$ -BTX and its replacement by proline, as in the  $\alpha 1$  sequence of species sensitive to  $\alpha$ -BTX, reduced the binding affinity by two orders of magnitude (Kasher et al., 2001). Moreover, replacement of <sup>HAP</sup>R188 by valine, which is invariant at this position in  $\alpha 1$ , resulted in a decrease of one order of magnitude in the affinity to  $\alpha$ -BTX (Kasher et al., 2001). The observation that  $\alpha 7$  of different species are highly homologous and the fact that even the mungoose  $\alpha 7$  binds  $\alpha$ -BTX (Ariel et al., 1998) clearly counter-indicate the use of the  $\alpha 7$  scaffold to study species-

specific resistance against  $\alpha$ -BTX. While the interaction of the  $\alpha 7$  peptide with  $\alpha$ -BTX is mostly by residues  $\alpha 7$ F189,  $\alpha 7$ Y190, and  $\alpha 7$ E191 (Moise et al., 2002), the interaction of  $\alpha 1$  with  $\alpha$ -BTX includes also residues at the base of  $\beta$  hairpin such as  $\alpha 1$ K185 and  $\alpha 1$ W187, the mutation of which confer resistance against  $\alpha$ -BTX (see below). Interestingly,  $^{HAP/\alpha 7}$ E191 interacts more extensively with  $\alpha$ -BTX in comparison to  $\alpha 1$ T191 and forms an electrostatic interaction with  $^B$ K38 (Figure 6A).

As shown in Figures 6A and 6C, the two HAP peptides (Harel et al., 2001; Scherf et al., 2001) are considerably shorter than  $\alpha 1^{182-202}$  and exhibit differences in the conformation and location of the tip of the  $\beta$  hairpin due to the one residue insertion and the  $\beta$  bulge in  $\alpha 1^{182-202}$ . The HAP peptides do not include K185 and H186, making  $^{HAP}$ W187 the positively charged N terminus. The  $\beta$  sheet interactions between  $\alpha 1$ H186- $\alpha 1$ W187 and  $\alpha 1$ L199- $\alpha 1$ D200 were not observed in the HAP, and the  $\beta$  hairpin is only 11 residues long in comparison to 15 residues in  $\alpha 1^{182-202}$ . Moreover, as a result of crystal packing forces, the position and orientation of  $^{HAP}$ W187 differ by as much as 3.9 Å between the two different monomers observed in the crystal structure of HAP with  $\alpha$ -BTX (Harel et al., 2001).

#### Comparison of the NMR-Derived Model with Earlier Site-Directed Mutagenesis Studies

A large number of residues within the 184–200 sequence have been implicated by various experimental methods as important for  $\alpha$ -BTX binding (Aronheim et al., 1988; Chaturvedi et al., 1993; Conti Tronconi et al., 1991; Levandoski et al., 1999; Spura et al., 1999). However, these studies were unable to reveal how the mutations influence toxin binding at the atomic-resolution level, and to determine whether the toxin affinity decreased due to side chain modification or due to change in conformation of the AChR peptides or segments. Our structure indicates that the side chains of residues  $\alpha 1$ K185,  $\alpha 1$ W187,  $\alpha 1$ Y189,  $\alpha 1$ Y190,  $\alpha 1$ T191,  $\alpha 1$ C192,  $\alpha 1$ P194, and  $\alpha 1$ Y198 interact directly with  $\alpha$ -BTX. On the other hand, the side chains of residues  $\alpha 1$ W184,  $\alpha 1$ H186,  $\alpha 1$ V188,  $\alpha 1$ C193,  $\alpha 1$ P197, and  $\alpha 1$ D200 do not contribute directly to  $\alpha$ -BTX binding.

Reduction of the disulfide bond did not decrease significantly the peptide affinity to  $\alpha$ -BTX. However, methylation of the free thiols decreased the affinity considerably (Kao and Karlin, 1986). This latter finding coincides with our results that indicate that  $\alpha 1$ C192 is directly involved in  $\alpha$ -BTX binding, whereas  $\alpha 1$ C193 and its disulfide bridge are not. Nevertheless, it should be stated that the disulfide bridge rigidifies the  $\beta$  hairpin tip and passively contributes to toxin affinity.

The NMR-derived model of the  $\alpha$ -BTX/AChR complex is in a remarkable agreement with pairwise interactions between AChR and the short  $\alpha$ -neurotoxin *Naja Mossambica Mossambica I* (*Nmm1*) revealed by double mutant cycle experiments (Malany et al., 2000; Osaka et al., 2000). The *Nmm1* R33 (homologous to  $^B$ R36, see Figure 7) was found to interact with  $^Y$ L119 and  $^Y$ W55, and a cation- $\pi$  interaction between  $^Y$ W55 and the *Nmm1* R33 was suggested (Osaka et al., 2000). In addition, *Nmm1* R33 was found to be coupled to  $\alpha 1$ W149,  $\alpha 1$ V188,  $\alpha 1$ Y190,  $\alpha 1$ Y198, and  $\alpha 1$ D200 of the  $\alpha 1$  subunit. It was thus

suggested that *Nmm1* R33 is inserted between the  $\alpha 1$  and  $\gamma$  subunits and anchors the  $\alpha$  toxin to the surfaces of both subunits (Malany et al., 2000), exactly as observed for  $^B$ R36 in our NMR-derived model of  $\alpha$ -BTX complex with AChR (see Figures 4A and 4B). Moreover, the *Nmm1* K27 (homologous to  $^B$ K26) was found to form strong electrostatic interaction with  $^Y$ E176 (see Figure 4E). Mutation of the *Nmm1* K47 (homologous to  $^B$ K52) decreased the affinity of the toxin to AChR by a factor of 400, and a weak interaction with  $^Y$ D174 was observed. The mutation of  $^Y$ E169 has not been tested. The above interactions observed by Taylor and coworkers are in excellent agreement with the interactions observed in our NMR-derived model (Table 2), attesting to the reliability of the modeling of the AChR  $\alpha 1$  and  $\gamma$  subunits in complex with  $\alpha$ -BTX. As stated earlier, such detailed analysis of the interactions between the heteropentameric AChR and  $\alpha$ -BTX was not possible using the superposition of  $\alpha$ -BTX on the crystal structure of AChBP which resulted in several clashes.

#### $^B$ R36 Is Invariant in Snake $\alpha$ -Neurotoxins

Sequence alignment of several long and short  $\alpha$ -neurotoxins displayed a high sequence identity (35%–65%) as well as five invariant cystine bridges (Figure 7). The alignment revealed that the arginine at the tip of the second finger,  $^B$ R36, and  $^B$ G37 are invariant (Figure 7). As mentioned earlier,  $^B$ R36 occupies the ACh binding site on the receptor, while the small and flexible  $^B$ G37 enables optimal fit of  $^B$ R36 in the ACh binding pocket. These findings are in excellent agreement with mutagenesis results that show that a mutation of R33 of *Nmm1* (homologous to  $^B$ R36, see Figure 7) results in four orders of magnitude decrease in the affinity of the toxin to AChR (Osaka et al., 2000). In addition to  $^B$ R36 and  $^B$ G37, residues  $^B$ W28 and  $^B$ P49 were the only invariant residues excluding the cysteines. Remarkably,  $^B$ W28 interacts extensively with the  $\gamma$  and  $\delta$  subunits.

#### $^B$ R36 Mimics the Interactions of ACh in the AChR Binding Site

The structural and chemical similarity between ACh and arginine makes it the best amino acid mimic of ACh (see Figure 4C). Therefore, the NMR-observed interactions of  $^B$ R36 in the ACh binding site and the additional ones found in the model are probably common to ACh. Photoaffinity labeling and mutational analysis of *Torpedo* AChR indicated that residues  $\alpha 1$ W86,  $\alpha 1$ Y93,  $\alpha 1$ W149,  $\alpha 1$ Y151,  $\alpha 1$ Y190,  $\alpha 1$ C192,  $\alpha 1$ C193, and  $\alpha 1$ Y198 from the  $\alpha 1$  subunit and  $^Y$ W55,  $^Y$ E57,  $^Y$ L109,  $^Y$ Y111,  $^Y$ Y117,  $^Y$ L119,  $^Y$ D174, and  $^Y$ E176 from the  $\gamma$  subunit contribute to ACh binding (Grutter and Changeux, 2001). As can be seen in Table 2, our NMR-derived model is in excellent agreement with these earlier predictions. These residues involved in ACh binding are highly conserved in all species to allow proper binding of ACh by enabling the cation- $\pi$  and hydrophobic interactions required for binding. Our NMR-derived model shows that both  $\alpha 1$ W149 and  $^Y$ W55 ( $^O$ W57 in the  $\delta$  subunit) form cation- $\pi$  interactions with the guanidinium group of  $^B$ R36. The cation- $\pi$  interaction between  $\alpha 1$ W149 and ACh was postulated by Dougherty and coworkers (Zhong et al., 1998). In the structure of AChBP, W143 (homologous to  $^O$ W149) was found to

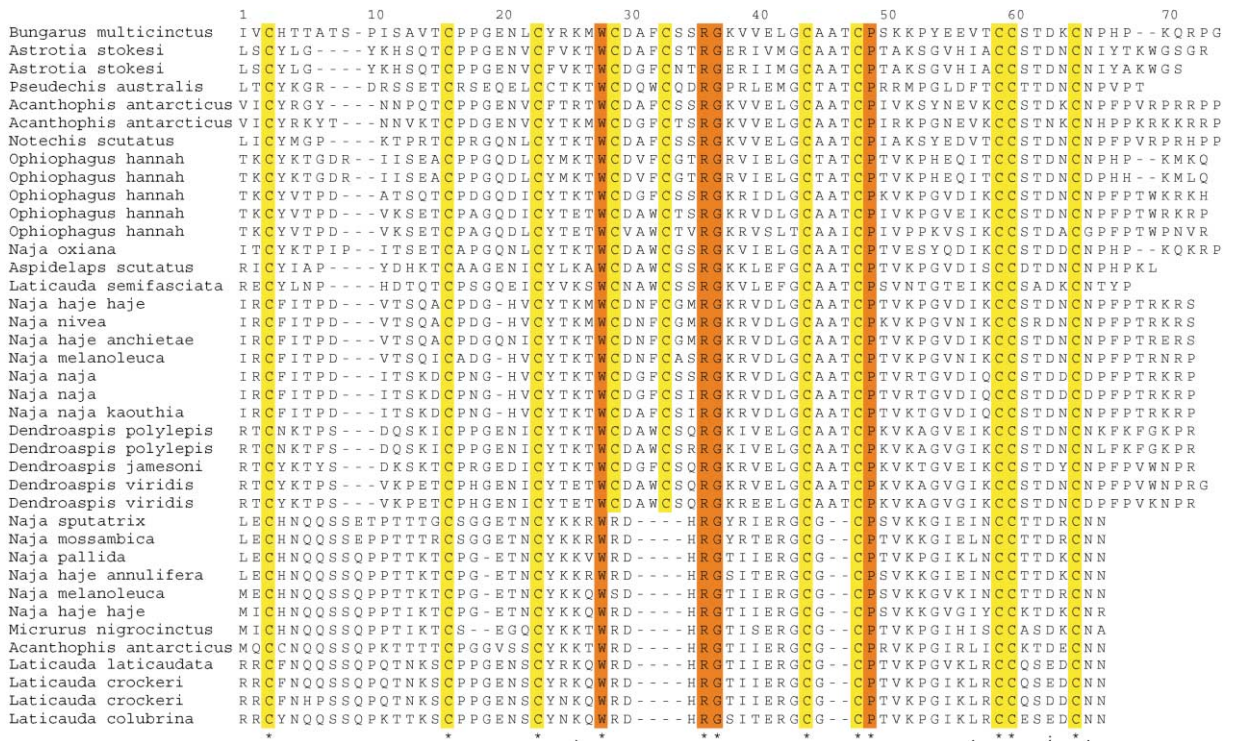


Figure 7. Sequence Alignment of Various  $\alpha$ -Neurotoxins  
Highlighted are the invariant cysteine residues (in yellow) and noncysteine residues (in orange).

form cation- $\pi$  interaction with a HEPES molecule that partially occupied the inferred ACh binding site (Brejc et al., 2001). A similar type of interaction was observed between W84 of ACh esterase and a quaternary ligand (Harel et al., 1993). A cation- $\pi$  interaction between  $^{\gamma}$ W55 and a neurotoxin arginine was suggested on the basis of double mutant cycle experiments (Osaka et al., 2000). We therefore conclude that the quaternary ammonium group of ACh forms cation- $\pi$  interactions with both  $^{\alpha 1}$ W149 and  $^{\gamma}$ W55, as does  $^{\beta}$ R36.

**The NMR Structure of  $\alpha$ -BTX Complex with  $\alpha 1^{182-202}$  Accounts for Species-Specific Susceptibility to the Toxin**

Snake neurotoxins have evolved to paralyze the snakes' prey by inactivating muscle AChR and therefore both long and short  $\alpha$ -neurotoxins exhibit high affinity to muscle AChR and its  $\alpha 1$  subunit. In Figure 8, sequences of the  $\alpha 1$  of various species are presented together with their relative binding affinity to  $\alpha$ -BTX. The natural preys of the snake *Bungarus multicinctus* are frogs and chicks, and it is therefore not surprising that  $\alpha$ -BTX binds lethally and with the highest affinity to their  $\alpha 1$ . The *Torpedo californica*  $\alpha 1$  sequence is similar to that of frogs and, therefore, exhibits similar affinities (Ohana and Gershoni, 1990). On the other hand, snakes themselves and their predators such as the mongoose are naturally resistant to snake venom in general, and  $\alpha$ -BTX in particular (Barchan et al., 1992). Other species such as humans and hedgehogs, the latter being closely related to the mongoose, exhibit reduced sensitivity to  $\alpha$ -BTX poisoning (Barchan et al., 1995). Understanding the influence

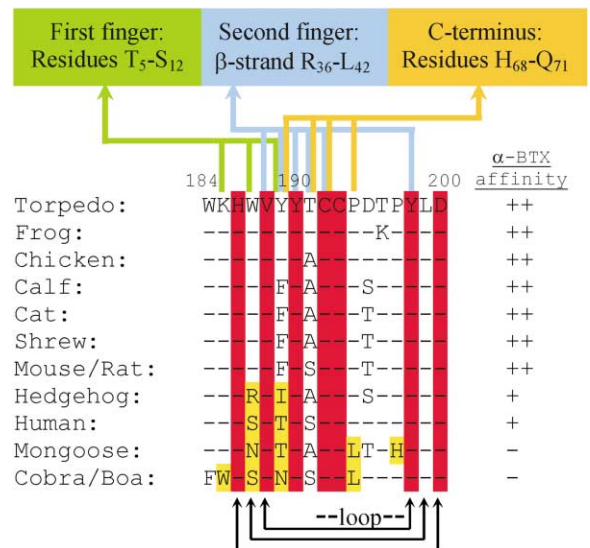


Figure 8. Sequence Comparison of  $\alpha 1$  of Different Species Showing the Segment 184–200

Affinities to  $\alpha$ -BTX are obtained from Ohana and Gershoni (1990), Conti-Tronconi et al. (1991), and Barchan et al. (1995).  $\alpha 1$  residues interacting with  $\alpha$ -BTX are marked with colored arrows and residues involved in the intramolecular  $\beta$  strand/ $\beta$  strand interactions are marked with black arrows. Conserved  $\alpha 1$  residues are colored red, and natural mutations leading to a decrease or abolition of  $\alpha$ -BTX affinity are in yellow.

of a mutation on the actual binding is a powerful tool in relating  $\alpha 1$  structure to its function.

The  $\beta$  hairpin  $\alpha^1$ K185- $\alpha^1$ D200 is the major  $\alpha 1$  subunit determinant involved in both ACh and snake toxin binding, protruding out of the  $\alpha 1$  subunit as a long tongue. While the upper and lower face of the  $\beta$  hairpin and the backbone of the N-terminal  $\beta$  strand ( $\alpha^1$ Y189- $\alpha^1$ T191) are involved in toxin binding (see Figure 2), only the lower face is involved directly in ACh binding. Resistance to snakes' toxins can therefore be obtained by mutating residues with side chains pointing to the upper face while conserving those with side chains pointing downwards and that are crucial for ACh binding. Figure 8 indicates that mutations of residues  $\alpha^1$ K185,  $\alpha^1$ W187,  $\alpha^1$ Y189,  $\alpha^1$ P194, and  $\alpha^1$ P197 lead to a decrease or loss of toxin binding capability. In snakes, resistance to  $\alpha$ -neurotoxins is conferred by the  $\alpha^1$ K185W,  $\alpha^1$ W187S,  $\alpha^1$ Y189N, and  $\alpha^1$ P194L mutations while in mongoose, resistance is obtained by  $\alpha^1$ W187N (putatively N-glycosylated),  $\alpha^1$ Y189T,  $\alpha^1$ P194L, and  $\alpha^1$ P197H mutations (Barchan et al., 1995). Our structure indicates that the side chains of residues  $\alpha^1$ K185,  $\alpha^1$ W187,  $\alpha^1$ Y189, and  $\alpha^1$ P194 point to the upper side of the  $\beta$  hairpin and interact extensively with  $\alpha$ -BTX. The aforementioned mutations obviate the favorable interactions with the toxin and abolish its binding. Figure 8 also indicates that mutations of residues  $\alpha^1$ D195 and  $\alpha^1$ T196 do not significantly alter the AChR affinity to the toxin. In susceptible species such as frogs,  $\alpha^1$ T196 is replaced by a lysine, whereas in cats,  $\alpha^1$ D195 is replaced by threonine. Interestingly,  $T_1$  relaxation time in the rotating frame ( $T_{1\rho}$ ) and rmsd values of residues  $\alpha^1$ D195 and  $\alpha^1$ T196 suggest they are more flexible than other residues within the binding determinant (Samson et al., unpublished data). Our findings suggest that these residues are solvent exposed in  $\alpha 1^{182-202}$  and do not contribute to  $\alpha$ -BTX binding. Finally, Figure 8 shows that residues  $\alpha^1$ H186,  $\alpha^1$ V188,  $\alpha^1$ Y190,  $\alpha^1$ C192,  $\alpha^1$ C193,  $\alpha^1$ Y198, and  $\alpha^1$ D200, which form the lower face of the  $\beta$  hairpin, are conserved. Four of these residues, namely,  $\alpha^1$ Y190,  $\alpha^1$ C192,  $\alpha^1$ C193,  $\alpha^1$ Y198, form the binding site for ACh and interact with  $^B$ R36, which mimics ACh.

The forms of AChR found in the brain, like  $\alpha 7$  as well as  $\alpha 2$ - $\alpha 6$ , are not the natural target for snake  $\alpha$ -neurotoxins as these toxins cannot cross the blood-brain barrier. The sequences of  $\alpha 7$  from different species are highly homologous and they strongly bind long neurotoxins but only weakly short neurotoxins. Mongoose resistance to  $\alpha$ -BTX developed by mutations in the  $\alpha 1$  segment 184-200 while its  $\alpha 7$  still binds  $\alpha$ -BTX and its sequence is highly homologous to those of mice and humans (Ariel et al., 1998).

## Conclusion

Our NMR-derived model for AChR-EC in complex with  $\alpha$ -BTX provides a convincing and complete explanation for  $\alpha$ -BTX binding and mode of inhibition of muscle AChR. The toxin forms a  $37^\circ$  angle with the tangent to the pentameric ring rather than being perpendicular, thus maximizing the contact area between  $\alpha$ -BTX and AChR. The extremely high affinity of the toxin to AChR is reconcilable with the large contact area of over  $1800 \text{ \AA}^2$ , dramatically larger than a contact of  $760 \text{ \AA}^2$  observed

in the AChBP superposition (Harel et al., 2001). The additional surface area observed in the AChR/ $\alpha$ -BTX complex is due to interactions between the  $\gamma/\delta$  subunits with  $\alpha$ -BTX third finger not observed in the AChBP superposition and more extensive interactions of the  $\alpha$ -BTX first finger with the  $\alpha 1$  subunit due to the longer  $\alpha 1$  determinant recognized by  $\alpha$ -BTX. Numerous interactions between AChR and  $\alpha$ -BTX are observed in the AChR model, and they agree very well with vast biochemical data obtained from photoaffinity labeling and site-directed mutagenesis. Due to clashes between  $\alpha$ -BTX and AChBP residues, such interactions could be only vaguely inferred from the AChBP superposition, and potential interactions with AChR could be deduced only by analogy to AChR. All data on species-specific resistance to  $\alpha$ -BTX are handsomely explained by the NMR structure of the  $\alpha 1$  peptide. This data could not be correlated with the structure of  $\alpha 7$ , the sequence of which is highly homologous among the different species. Finally, the critical role suggested in our study for  $^B$ R36 is in perfect agreement with its conservation throughout the  $\alpha$ -neurotoxin family (Figure 7). It is not only that the  $\alpha$ -BTX second finger serves as a mechanical lid, preventing ACh from entering and leaving the binding pocket (Harel et al., 2001). Rather, the  $\alpha$ -neurotoxin-conserved R36 mimics ACh in its binding pocket and forms cation- $\pi$  interactions with both  $^W$ W149 and  $^W$ W55/ $^W$ W57 of the AChR.

## Experimental Procedures

### NMR Sample Preparation

The peptide, EERGWKHWVYYTCCPDTPYLDITEE ( $\alpha 1^{182-202}$ ), corresponding to residues 182-202 of the  $\alpha 1$  of *Torpedo californica* and elongated with two glutamic residues at each terminus to increase solubility, was synthesized and purified as previously described (Samson et al., 2001).  $\alpha$ -BTX was purchased from Sigma. The  $\alpha$ -BTX/ $\alpha 1^{182-202}$  complex was prepared and purified as described earlier. The purified and lyophilized complex was dissolved in 90%  $\text{H}_2\text{O}/10\%$   $\text{D}_2\text{O}$  and 0.05%  $\text{NaN}_3$  and acidified with HCl to pH 4. Final concentration of the complex in the NMR sample was 2 mM. For measurements in  $\text{D}_2\text{O}$ , the lyophilized  $\alpha$ -BTX/ $\alpha 1^{182-202}$  complex was dissolved in 99.8%  $\text{D}_2\text{O}$ , incubated at  $42^\circ\text{C}$  for 14 hr, and lyophilized again. The complex was then redissolved in 99.99%  $\text{D}_2\text{O}$  and acidified to pH 4 using  $d_4$ -acetic acid.

### NMR Measurements

NOESY spectra with 8K data points in  $F_2$  and 800 increments in  $F_1$  were acquired with mixing times of 40 and 150 ms in 90%  $\text{H}_2\text{O}/10\%$   $\text{D}_2\text{O}$  and in  $\text{D}_2\text{O}$ . States-TPPI method was used for phase sensitivity and the WATERGATE (WATER suppression by gradient-tailored excitation) or 3-19-9 sequences were used for water suppression in the  $\text{H}_2\text{O}$  sample (Piotto et al., 1992; Sklenar et al., 1993). A double-quantum filtered correlation spectroscopy (DQF-COSY) spectrum was acquired in  $\text{D}_2\text{O}$  using presaturation of the HDO resonance. All spectra were acquired at  $37^\circ\text{C}$  on Bruker DMX-500 and DRX-800 spectrometers and then processed and analyzed using Bruker's XWINNMR and AURELIA software packages (Neidig et al., 1995).

### Experimental Constraints

The calibration curve for distance restraints in the amide and aromatic regions was based on the intensity of sequential  $\text{H}^{\alpha}(i)/\text{H}^{\alpha}(i+1)$  crosspeaks of residues involved in  $\beta$  sheet, corresponding to a distance of 2.2  $\text{Å}$ . The cross peak intensities of the  $\text{H}^{\alpha}/\text{H}^{\alpha}$  interstrand NOEs in  $\beta$  sheets, corresponding to a 2.3  $\text{Å}$  distance, were used as a reference for NOE distances in the aliphatic region of the spectrum recorded in 99.99%  $\text{D}_2\text{O}$ . The upper bound distance constraints were 130% of the NOE-derived distances to account for internal motion and proton multiplicity (Roberts, 1993), and the lower bound

distance was set to 1.8 Å. Dihedral angle restraints were determined using the  $^3J_{\text{HNH}\alpha}$  couplings. The  $\phi$  angles of residues with a coupling constant smaller than 6 Hz were constrained to  $-65^\circ \pm 20^\circ$ , and the  $\phi$  angles of residues with a  $^3J_{\text{HNH}\alpha}$  larger than 8 Hz were constrained to  $-120^\circ \pm 20^\circ$ .  $^3J_{\text{HNH}\alpha}$  values between 6 and 8 Hz were regarded as uninformative (Roberts, 1993). For each of the six disulfide bonds,  $^{\text{B}}\text{C}3/\text{C}23$ ,  $^{\text{B}}\text{C}16/\text{C}44$ ,  $^{\text{B}}\text{C}29/\text{C}33$ ,  $^{\text{B}}\text{C}48/\text{C}59$ ,  $^{\text{B}}\text{C}60/\text{C}65$ , and  $^{\text{B}}\text{C}192/\text{C}193$ ,  $d_{\text{S}\gamma\text{-S}\gamma}$  was constrained between 2.01 and 2.03 Å. Two constraints were applied for each hydrogen bond; the H...O distance was constrained between 1.8 and 2.3 Å and the corresponding N...O distance between 2.5 and 3.3 Å. The information regarding  $^3J_{\text{H}\alpha\text{H}\beta}$  couplings,  $\text{H}^\alpha/\text{H}^\beta$ , and  $\text{H}^\alpha/\text{H}^\beta$  crosspeak intensities was utilized for stereospecific assignment (Wagner et al., 1987). The intensities of the  $\text{H}^\alpha/\text{H}^\beta$  and  $\text{H}^\alpha/\text{H}^\beta$  crosspeaks were measured from NOESY spectra recorded with a mixing time of 40 ms. The  $\chi_1$  angles were constrained to either  $60^\circ \pm 30^\circ$ ,  $-60^\circ \pm 30^\circ$ , or  $180^\circ \pm 30^\circ$ .

#### Structure Calculation

Structure calculations were performed on a Silicon Graphics OC-TANE workstation with version 1.0 of the CNS program using the NMR-derived distance and dihedral angle constraints (Brünger et al., 1998). Structures were generated with a hybrid distance geometry-dynamical simulated annealing method. The structure calculations were accomplished in an iterative manner. Initial input list included only  $\text{H}^\alpha/\text{H}^\beta$  and  $\text{H}^\alpha/\text{H}^\beta$  distance restraints, dihedral angle restraints, and few unambiguous hydrogen bond constraints derived from the predetermined secondary structure elements (Samson et al., 2001). The preliminary structures were used to complete assignment of ambiguous NOE peaks and deduce possible oxygen acceptors for slowly exchanging labile hydrogens. This cycle was repeated with gradual addition of aromatic constraints,  $\beta$  proton constraints, and side chain constraints. The structures were displayed for analysis using RasMol Molecular Renderer and MOLMOL (Spectrospin AG) programs (Koradi et al., 1996).

#### Homology Modeling and Docking

The AChBP sequence was aligned with those of 50  $\alpha 1$  of various species obtained from the Swiss-Prot databank using the ClustalW program (Thompson et al., 1994). The same process was repeated for the  $\beta$ ,  $\gamma$ , and  $\delta$  subunits. A single AChBP subunit consisting of 210 amino acids served as a template for our model. Each subunit of the AChR model was therefore delimited to this size and the following segments,  $\alpha 1(2-211)$ ,  $\delta(2-225)$ ,  $\gamma(2-219)$ , and  $\beta(2-217)$ , corresponding to the 210 residue subunit of AChBP, were modeled. Inserts in the  $\delta$ ,  $\gamma$ , and  $\beta$  sequences increase the length of the respective subunit. For most of the sequence, the alignment was straightforward requiring no insertion or deletions. These segments were considered structurally conserved regions, in which the conformation of the polypeptide chain is unchanged. Random loops were generated where insertion or deletions occurred using the Homology module in the Accelrys package. No backbone-backbone clashes were observed. Side chains exhibiting steric clashes with other side chain or backbone atoms were manually assigned with an alternative rotamer conformation. The loops' conformations were refined using molecular dynamics calculations, whereas the rest of the model was fixed at the initial coordinates. To dock two  $\alpha$ -BTX molecules into the AChR model,  $\alpha 1^{182-202}$  residues 185-190 and 198-199 from the NMR structure of the  $\alpha$ -BTX/ $\alpha 1^{182-202}$  complex were superimposed on the corresponding residues in the AChR model, resulting in an rmsd of 1.4 Å. Residues  $\alpha 1^{185-202}$  of the nascent  $\alpha 1$  model were assigned with the cartesian coordinates of the corresponding  $\alpha 1^{182-202}$  segment of the complex, and two  $\alpha$ -BTX molecules were introduced in their peptide bound state. The replacement of the  $\beta$  hairpin in the initial AChR model with the  $\beta$  hairpin of  $\alpha 1^{182-202}$  bound to  $\alpha$ -BTX created a discontinuity at positions  $^{\text{K}}185$  and  $^{\text{D}}200$ , which was resolved by a few steps of dynamics and minimization. The side chain of  $^{\text{S}}34$  in the two docked toxin molecules collided with the  $\delta$  and  $\gamma$  subunits and its conformation was modified by molecular dynamics calculations applied only to residues  $^{\text{B}}\text{C}33$ - $^{\text{B}}\text{S}35$ .

#### Acknowledgments

We thank Mrs. Aviva Kapitkovski and Mr. Yehezkiel Haik for synthesis and purifying the AChR peptides. This study was supported

by a US-Israel Binational Science Foundation grant 98-328 to J.A. J.A. is the Dr. Joseph and Ruth Owades Professor of Chemistry.

Received: January 22, 2002

Revised: May 29, 2002

#### References

- Ariel, S., Asher, O., Barchan, D., Ovadia, M., and Fuchs, S. (1998). The mongoose neuronal acetylcholine receptor ( $\alpha 7$ ) binds  $\alpha$ -bungarotoxin. *Ann. NY Acad. Sci.* 841, 93-96.
- Aronheim, A., Eshel, Y., Mosckovitz, R., and Gershoni, J.M. (1988). Characterization of the binding of  $\alpha$ -bungarotoxin to bacterially expressed cholinergic binding sites. *J. Biol. Chem.* 263, 9933-9937.
- Barchan, D., Kachalsky, S., Neumann, D., Vogel, Z., Ovadia, M., Kochva, E., and Fuchs, S. (1992). How the mongoose can fight the snake: the binding site of the mongoose acetylcholine receptor. *Proc. Natl. Acad. Sci. USA* 89, 7717-7721.
- Barchan, D., Ovadia, M., Kochva, E., and Fuchs, S. (1995). The binding site of the nicotinic acetylcholine receptor in animal species resistant to  $\alpha$ -bungarotoxin. *Biochemistry* 34, 9172-9176.
- Basus, V.J., Billeter, M., Love, R.A., Stroud, R.M., and Kuntz, I.D. (1988). Structural studies of  $\alpha$ -bungarotoxin. 1. Sequence-specific  $^1\text{H}$  NMR resonance assignments. *Biochemistry* 27, 2763-2771.
- Basus, V.J., Song, G., and Hawrot, E. (1993). NMR solution structure of an  $\alpha$ -bungarotoxin/nicotinic receptor peptide complex. *Biochemistry* 32, 12290-12298.
- Blount, P., and Merlie, J.P. (1989). Molecular basis of the two non-equivalent ligand binding sites of the muscle nicotinic acetylcholine receptor. *Neuron* 3, 349-357.
- Brejč, K., van Dijk, W.J., Klaassen, R.V., Schuurmans, M., van Der Oost, J., Smit, A.B., and Sixma, T.K. (2001). Crystal structure of an ACh-binding protein reveals the ligand-binding domain of nicotinic receptors. *Nature* 411, 269-276.
- Brünger, A.T., Adams, P.D., Clore, G.M., DeLano, W.L., Gros, P., Grosse-Kunstleve, R.W., Jiang, J.S., Kuszewski, J., Nilges, M., Pannu, N.S., et al. (1998). Crystallography & NMR system: A new software suite for macromolecular structure determination. *Acta Crystallogr. D Biol. Crystallogr.* 54, 905-921.
- Chaturvedi, V., Donnelly-Roberts, D.L., and Lentz, T.L. (1993). Effects of mutations of Torpedo acetylcholine receptor  $\alpha 1$  subunit residues 184-200 on  $\alpha$ -bungarotoxin binding in a recombinant fusion protein. *Biochemistry* 32, 9570-9576.
- Conti Tronconi, B.M., Diethelm, B.M., Wu, X.D., Tang, F., Bertazzon, T., Schroder, B., Reinhardt-Maelicke, S., and Maelicke, A. (1991).  $\alpha$ -bungarotoxin and the competing antibody WF6 interact with different amino acids within the same cholinergic subsite. *Biochemistry* 30, 2575-2584.
- Corringer, P.J., Le Novère, N., and Changeux, J.P. (2000). Nicotinic receptors at the amino acid level. *Annu. Rev. Pharmacol. Toxicol.* 40, 431-458.
- Grotter, T., and Changeux, J.P. (2001). Nicotinic receptors in wonderland. *Trends Biochem. Sci.* 26, 459-463.
- Haggerty, J.G., and Froehner, S.C. (1981). Restoration of 125I- $\alpha$ -bungarotoxin binding activity to the  $\alpha$ -subunit of Torpedo acetylcholine receptor isolated by gel electrophoresis in sodium dodecyl sulfate. *J. Biol. Chem.* 256, 8294-8297.
- Harel, M., Schalk, I., Ehret-Sabatier, L., Bouet, F., Goeldner, M., Hirth, C., Axelsen, P.H., Silman, I., and Sussman, J.L. (1993). Quaternary ligand binding to aromatic residues in the active-site gorge of acetylcholinesterase. *Proc. Natl. Acad. Sci. USA* 90, 9031-9035.
- Harel, M., Kasher, R., Nicolas, A., Guss, J.M., Balass, M., Fridkin, M., Smit, A.B., Brejč, K., Sixma, T.K., Katchalski-Katzip, E., et al. (2001). The binding site of acetylcholine receptor as visualized in the X-ray structure of a complex between  $\alpha$ -bungarotoxin and a mimotope peptide. *Neuron* 32, 265-275.
- Kao, P.N., and Karlin, A. (1986). Acetylcholine receptor binding site contains a disulfide cross-link between adjacent half-cystinyl residues. *J. Biol. Chem.* 261, 8085-8088.

- Karlin, A. (1993). Structure of nicotinic acetylcholine receptors. *Curr. Opin. Neurobiol.* **3**, 299–309.
- Kasher, R., Balass, M., Scherf, T., Fridkin, M., Fuchs, S., and Katchalski-Katzir, E. (2001). Design and synthesis of peptides that bind  $\alpha$ -bungarotoxin with high affinity. *Chem. Biol.* **8**, 147–155.
- Koradi, R., Billeter, M., and Wüthrich, K. (1996). MOLMOL: a program for display and analysis of macromolecular structures. *J. Mol. Graph.* **14**, 29–32, 51–55.
- Levandoski, M.M., Lin, Y., Moise, L., McLaughlin, J.T., Cooper, E., and Hawrot, E. (1999). Chimeric analysis of a neuronal nicotinic acetylcholine receptor reveals amino acids conferring sensitivity to alpha-bungarotoxin. *J. Biol. Chem.* **274**, 26113–26119.
- Malany, S., Osaka, H., Sine, S.M., and Taylor, P. (2000). Orientation of  $\alpha$ -neurotoxin at the subunit interfaces of the nicotinic acetylcholine receptor. *Biochemistry* **39**, 15388–15398.
- Moise, L., Piserchio, A., Basus, V.J., and Hawrot, E. (2002). NMR structural analysis of  $\alpha$ -bungarotoxin and its complex with the principal  $\alpha$ -neurotoxin-binding sequence on the  $\alpha 7$  subunit of a neuronal nicotinic acetylcholine receptor. *J. Biol. Chem.* **277**, 12406–12417.
- Neidig, K.-P., Geyer, M., Gorler, A., Antz, C., Saffrich, R., Beneicke, W., and Kalbitzer, H. (1995). AURELIA, a program for computer-aided analysis of multidimensional NMR spectra. *J. Biomol. NMR* **6**, 255–270.
- Ohana, B., and Gershoni, J.M. (1990). Comparison of the toxin binding sites of the nicotinic acetylcholine receptor from *Drosophila* to human. *Biochemistry* **29**, 6409–6415.
- Osaka, H., Malany, S., Molles, B.E., Sine, S.M., and Taylor, P. (2000). Pairwise electrostatic interactions between  $\alpha$ -neurotoxins and  $\gamma$ ,  $\delta$ , and  $\epsilon$ -subunits of the nicotinic acetylcholine receptor. *J. Biol. Chem.* **275**, 5478–5484.
- Piotto, M., Saudek, V., and Sklenar, V. (1992). Gradient-tailored excitation for single-quantum NMR spectroscopy of aqueous solutions. *J. Biomol. NMR* **2**, 661–665.
- Roberts, G.C.K. (1993). *NMR of Macromolecules*, D. Rickwood and B.D. Hames, eds. (New York: Oxford University Press).
- Samson, A.O., Chill, J.H., Rodriguez, E., Scherf, T., and Anglister, J. (2001). NMR mapping and secondary structure determination of the major acetylcholine receptor  $\alpha$ -subunit determinant interacting with  $\alpha$ -bungarotoxin. *Biochemistry* **40**, 5464–5473.
- Scarselli, M., Spiga, O., Ciutti, A., Bernini, A., Bracci, L., Lelli, B., Lozzi, L., Calamandrei, D., Di Maro, D., Klein, S., and Niccolai, N. (2002). NMR structure of  $\alpha$ -bungarotoxin free and bound to a mimotope of the nicotinic acetylcholine receptor. *Biochemistry* **41**, 1457–1463.
- Scherf, T., Balass, M., Fuchs, S., Katchalski-Katzir, E., and Anglister, J. (1997). Three-dimensional solution structure of the complex of  $\alpha$ -bungarotoxin with a library-derived peptide. *Proc. Natl. Acad. Sci. USA* **94**, 6059–6064.
- Scherf, T., Kasher, R., Balass, M., Fridkin, M., Fuchs, S., and Katchalski-Katzir, E. (2001). A  $\beta$ -hairpin structure in a 13-mer peptide that binds  $\alpha$ -bungarotoxin with high affinity and neutralizes its toxicity. *Proc. Natl. Acad. Sci. USA* **98**, 6629–6634.
- Servent, D., Mourier, G., Antil, S., and Menez, A. (1998). How do snake curaremimetic toxins discriminate between nicotinic acetylcholine receptor subtypes. *Toxicol. Lett.* **102–103**, 199–203.
- Sklenar, V., Piotto, M., Leppik, R., and Saudek, V. (1993). *J. Magn. Reson. A* **102**, 241–245.
- Spura, A., Russin, T.S., Freedman, N.D., Grant, M., McLaughlin, J.T., and Hawrot, E. (1999). Probing the agonist domain of the nicotinic acetylcholine receptor by cysteine scanning mutagenesis reveals residues in proximity to the  $\alpha$ -bungarotoxin binding site. *Biochemistry* **38**, 4912–4921.
- Thompson, J.D., Higgins, D.G., and Gibson, T.J. (1994). CLUSTAL W: improving the sensitivity of progressive multiple sequence alignment through sequence weighting, positions-specific gap penalties and weight matrix choice. *Nucleic Acids Res.* **22**, 4673–4680.
- Tsetlin, V. (1999). Snake venom  $\alpha$ -neurotoxins and other 'three-finger' proteins. *Eur. J. Biochem.* **264**, 281–286.
- Wagner, G., Braun, W., Havel, T.F., Schaumann, T., Go, N., and Wüthrich, K. (1987). Protein structures in solution by nuclear magnetic resonance and distance geometry. The polypeptide fold of the basic pancreatic trypsin inhibitor determined using two different algorithms, DISGEO and DISMAN. *J. Mol. Biol.* **196**, 611–639.
- Wilson, P.T., Hawrot, E., and Lentz, T.L. (1988). Distribution of  $\alpha$ -bungarotoxin binding sites over residues 173–204 of the  $\alpha$ -subunit of the acetylcholine receptor. *Mol. Pharmacol.* **34**, 643–650.
- Wüthrich, K. (1986). *NMR of Proteins and Nucleic Acids* (New York: Wiley).
- Zeng, H., Moise, L., Grant, M.A., and Hawrot, E. (2001). The solution structure of the complex formed between  $\alpha$ -bungarotoxin and an 18mer cognate peptide derived from the  $\alpha 1$  subunit of the nicotinic acetylcholine receptor from *torpedo californica*. *J. Biol. Chem.* **276**, 22930–22940.
- Zhong, W., Gallivan, J.P., Zhang, Y., Li, L., Lester, H.A., and Dougherty, D.A. (1998). From ab initio quantum mechanics to molecular neurobiology: a cation- $\pi$  binding site in the nicotinic receptor. *Proc. Natl. Acad. Sci. USA* **95**, 12088–12093.

#### Accession Numbers

The atomic coordinates of the energy-minimized average coordinates of the  $\alpha$ -BTX/ $\alpha 1^{182-202}$  complex (1L4W), the 20 lowest energy NMR structures (1LJZ), and the NMR-derived model of the  $\alpha$ -BTX/AChR-EC complex (1LK1) have been deposited in the Protein Data Bank.